International Journal of Mechanical, Industrial and Aerospace Sciences
ISSN: 2517-9950
Vol:6, No:12, 2012

State Dependent Riccati Equation Based Roll Autopilot for 122mm Artillery Rocket

Muhammad Kashif Siddiq, Fang Jian Cheng, and Yu Wen Bo

***Abstract*—**State-dependent Riccati equation based controllers are becoming increasingly popular because of having attractive properties like optimality, stability and robustness. This paper focuses on the design of a roll autopilot for a fin stabilized and canard controlled 122mm artillery rocket using state-dependent Riccati equation technique. Initial spin is imparted to rocket during launch and it quickly decays due to straight tail fins. After the spin phase, the roll orientation of rocket is brought to zero with the canard deflection commands generated by the roll autopilot. Roll autopilot has been developed by considering uncoupled roll, pitch and yaw channels. The canard actuator is modeled as a second-order nonlinear system. Elements of the state weighing matrix for Riccati equation have been chosen to be state dependent to exploit the design flexibility offered by the Riccati equation technique. Simulation results under varying conditions of flight demonstrate the wide operating range of the proposed autopilot.

***Keywords*—**Fin stabilized 122mm artillery rocket, Roll Autopilot, Six degree of freedom trajectory model, State-dependent Riccati equation.

I. Introduction

ROLL autopilot design for guided artillery rockets that can ensure stable performance over the full flight envelope is a challenging task primarily because of flexible nature of the airframe, cross coupling, uncertainty in aerodynamic parameters, external disturbances, and inaccuracies in measurements obtained from onboard sensors. As per the conventional practice of classical linear control techniques, dynamic models of rockets are linearized around several operating points in flight envelope and then the gain scheduled autopilots are designed. However, the performance of these classical autopilots can only be guaranteed within a narrow range of variations in flight conditions and model uncertainties. This has necessitated the application of nonlinear control techniques in order to maintain the operability of controllers over a wider range of operating conditions.

The advent of powerful low-cost micro-processors has equipped the designers with an effective tool to meet the challenges in applications of nonlinear control. The most recent applications, particularly in aerospace and military applications, now demand stringent accuracy and cost requirements in nonlinear control systems. This has expedited the development of nonlinear control theory for application to challenging, complex, dynamical real-world problems, particularly those that bear major practical significance in military industries. Researchers are striving to develop control algorithms that are simple, and yet produce optimal performance in the sense of control effort and state errors.

State-dependent Riccati equation (SDRE) control is a highly promising and very attractive practical tool for obtaining approximate solutions to infinite-time horizon nonlinear optimal control problems in feedback form. The SDRE method provides an attractive alternative to solving the Hamilton Jacobi Bellman partial differential equation, allowing for the systematic and effective design of nonlinear feedback controllers for a variety of applications. The potential of this method is characterized by possessing the crucial features of stability, optimality, real-time implementation, and inherent robustness with respect to parametric uncertainties.

Although application potential of the SDRE nonlinear control technique in practical nonlinear control problems is well recognized, the industry acceptance of the technique has not been appreciable. The main reasons for this being the SDRE approach requires advanced numerical methods for its implementation, and the perception that this technique may not be computationally feasible for real-time implementation on commercial off-the-shelf processors. P. K. Menon *et al* [1], using software based on the Schur algorithm and the Kleinman method, showed that SDRE control laws can be implemented at speeds up to 2 kHz sample rates using commercial off-the-shelf processors, for problems of the size commonly encountered in missile flight control applications. The potential of SDRE technique for flight control applications has been demonstrated by researchers in [2]–[9]. Cimen provided a comprehensive overview of the present state of the art of SDRE control technique in [10] and [11], and addressed the systematic design of nonlinear controllers via SDRE method in [12]. Controllability and stability issues of SDRE technique are well addressed in [13]–[17].

This paper focuses on the design of a SDRE based roll autopilot for a canard controlled 122mm artillery rocket. The rocket having front canards and folded straight tail fins is given initial spin at the time of launch. Tails fins are deployed immediately after launch and offer high roll damping moment thereby reducing the spin rate to zero within six seconds of flight. The canards are then deployed and the roll orientation of rocket is regulated to zero with the canard deflection

Muhammad Kashif Siddiq is Ph.D student in Beijing University of Aeronautics and Astronautics, Beijing, 100083 China (phone: 0086-13436479484; e-mail: kashif_s4u@ hotmail.com).

Fang Jian Cheng is Professor in Instrumentation Science and Opto-electronics Engineering Department of Beijing University of Aeronautics and Astronautics, Beijing, 100083 China (e-mail: fangjiancheng@ buaa.edu.cn).

Yu Wen Bo is Associate Professor in Instrumentation Science and Opto-electronics Engineering Department, Beijing University of Aeronautics and Astronautics, Beijing, 100083 China (e-mail: yuwenbo@buaa.edu.cn).

commands generated by the SDRE based roll autopilot. The designed controller produces promising results for the subject application. Extensive simulations have been carried out and the results corrugate the efficacy of the proposed autopilot over a wide range of flight conditions.

II. SDRE Control Methodology

A. SDRE Problem Formulation

Consider the autonomous, infinite-horizon, nonlinear regulator problem for minimizing the performance index

$$J=\frac{1}{2}\int_0^\infty \left(x^T(t)Q(x)x(t)+u^T(t)R(x)u(t)\right)dt \tag{1}$$

with respect to the state x and control u subject to the nonlinear differential constraints:

$$\dot{x}(t)=f(x)+B(x)u(t),\quad x(0)=x_0 \tag{2}$$

where $Q(x) \geq 0$ *(positive definite)* and $R(x) > 0$ (semi-positive definite) for all x and where

Condition 1. $f(x)$ is a continuously differentiable function of x, i.e.

$$f(x)\in C^1 \tag{3}$$

Condition 2

$$f(0)=0 \tag{4}$$

Under the specified conditions, a control law

$$u(x)=k(x)=-K(x)x,\quad k(0)=0 \tag{5}$$

is sought that (approximately) minimizes the cost function in (1) subject to the input affine nonlinear differential constraint in (2) while regulating the system to the origin for all x, such that $lim_{t\to\infty}x(t) = 0$. This is the basic idea of the SDRE method for nonlinear regulation [10].

B. SDRE Controller Structure

The SDRE approach as outlined in [10] and [18] for obtaining a suboptimal, locally asymptotically stabilizing solution of (1) and (2) is:

1) Use direct parameterization to factorize nonlinear system dynamics into a linear like structure which contains the state-dependent coefficient (SDC) matrices

2)
$$\dot{x}(t)=A(x)x(t)+B(x)u(t),\quad x(0)=x_0 \tag{6}$$

where

$$f(x)=A(x)x \tag{7}$$

If the condition, $f(x) \in C1$, is satisfied then there is an infinite number of ways to factor $f(x)$ into $A(x)x$ and that $A(x)$ can be parameterized as $A(x,\alpha)$, where α is a vector of free design parameters. In order to obtain a valid solution of the SDRE, the pair $\{A(x, \alpha), B(x)\}$ must meet the condition of point wise stability in the linear sense for all x in the domain of interest.

3) Solve the algebraic state-dependent Riccati equation

$$\begin{aligned}&A^T(x)P(x)+P(x)A(x)\\&-P(x)B(x)R^{-1}(x)B^T(x)P(x)+Q(x)=0\end{aligned} \tag{8}$$

to obtain $P(x) \geq 0$. $P(x)$ is the unique, symmetric, positive-definite solution of the algebraic state-dependent Riccati equation i.e. (8), and hence the name SDRE control.

4) The nonlinear feedback controller equation is given by

5)
$$u(x)=-R^{-1}(x)B^T(x)P(x)x \tag{9}$$

and the resulting SDRE controlled trajectory is the solution of the quasi-linear closed-loop dynamics

$$\dot{x}(t)=\left[A(x)-B(x)R^{-1}(x)B^T(x)P(x)\right]x(t) \tag{10}$$

The SDC matrix for the closed loop dynamics is

$$A_{CL}(x)=A(x)-B(x)K(x) \tag{11}$$

and the state feedback gain for minimizing the cost function (1) is

$$K(x)=R^{-1}(x)B^T(x)P(x) \tag{12}$$

The SDRE solution to (1) and (2) is a true generalization of the infinite-horizon time-invariant linear quadratic regulator (LQR) problem, where all of the coefficient matrices are state-dependent. At each instant of computing the control action, the method treats the state-dependent coefficient matrices as being constant, and computes a control action by solving a linear quadratic optimal control problem. As is evident from (8), the resulting controller relies on a solution, point wise in R^n, of an algebraic Riccati equation thereby leading to the SDRE terminology.

If the coefficient and weighting matrices are selected as constant, the nonlinear regulator problem becomes the LQR problem and the SDRE control method matches the steady-state linear regulator.

In order to perform tracking / command following, the SDRE controller can be implemented as an integral servo-mechanism as explained and demonstrated in [3],[10], and [18]. The procedure is outlined here briefly. The state x is decomposed as

$$x = \begin{bmatrix} x_T \\ x_N \end{bmatrix} \tag{13}$$

where it is desired for the vector components of x_T to track a reference command r_c. Augment the state vector x with x_I, the integral states of x_T:

$$\tilde{x} = \begin{bmatrix} x_I \\ x_T \\ x_N \end{bmatrix} \tag{14}$$

The augmented system is given by

$$\dot{\tilde{x}} = \tilde{A}(\tilde{x},\alpha)\tilde{x} + \tilde{B}(\tilde{x})u \tag{15}$$

where

$$\dot{\tilde{x}} = \tilde{A}(\tilde{x},\alpha) = \begin{bmatrix} 0 & \mathrm{I} \vdots 0 \\ 0 & A(x,\alpha) \end{bmatrix}, \quad \tilde{B}(\tilde{x}) = \begin{bmatrix} 0 \\ B(x) \end{bmatrix} \tag{16}$$

and the SDRE integral servo controller is given by

$$u = -\tilde{R}^{-1}(\tilde{x})\tilde{B}^T(\tilde{x})\tilde{P}(\tilde{x}) \begin{bmatrix} x_I - \int r_c dt \\ x_T - r_c \\ x_N \end{bmatrix} \tag{17}$$

C. SDC Parameterization

There are many systems that do not conform to the structure or conditions given in (2) to (4) and the SDRE technique cannot be directly applied. In these cases, there is an art in converting the given system to a conforming system so that an effective SDRE design can be carried out. References [11] and [18] present several cases where the system is non-conforming, and show in each case how to convert the system to a conforming one.

D. Selection of Q and R Matrices

The solution to the Riccati Equation depends on selection of the state and control weighting matrices Q and R, respectively. Q is a matrix of weighting coefficients used to penalize any state from becoming too large. Similarly, R is used to penalize the control action to remain within bounds. These matrices are design parameters that also affect the overall performance of the closed loop system. A remarkable design flexibility offered by SDRE approach is that by penalizing the appropriate states or control action, the designer can set constraints on the system. Elements of Q and R matrices should be selected such that the corresponding states and inputs which should be restrained from becoming arbitrarily large, are penalized the most. From simple to complicated, the elements of matrices Q and R can simply be constant or can be chosen as functions of states with their values varying throughout the control process depending upon the state values. Reference [12] proposed a procedure for selecting the state dependent elements of Q and R matrices. Although there are no rigorous methods for selecting these matrices, some guidelines for their selection based on good practices as mentioned in [19] are useful.

III. Rocket Configuration

Rocket configuration being studied has following salient features:

1) Rocket comes out of launch tube with spin rate of 5.8 revolutions per second.
2) Fixed tail having straight fins as shown in Fig. 1. Rear view of the rocket is shown in Fig. 2. The tail fins open up once the rocket comes out of launch tube/canister. These straight fins provide a high roll damping moment and retard the spin rate of rocket body.
3) Deployable canards for control purposes. During launch, canards remain folded inside rocket body and are deployed only after 6 seconds of launch.

The main physical parameters of the subject artillery rocket are summarized in Table I. The rocket leaves the muzzle with initial spin rate of 5.8 revolutions per second. This initial spin mitigates the effects of mass and configuration asymmetries. The straight tail fins offer high roll damping moment and the spin rate of rocket reduces to zero within first six seconds of flight. Canards are deployed at the time of six seconds after launch and are used to bring the roll orientation of rocket to zero, later these canards can be used for aerodynamic maneuvering to facilitate guidance and control of the rocket.

Fig. 1 Canard controlled 122mm rocket with straight tail fins

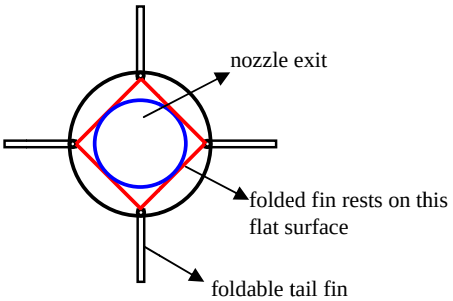

Fig. 2 Rear view of the rocket

TABLE I
PHYSICAL PARAMETERS OF 122MM ARTILLERY ROCKET

Rocket Parameters	Value
caliber	122mm
overall length	2.87m
total mass	66.0kg
propellant mass	20.5kg
propellant burning time	1.67s
mean thrust	23600N
initial center of gravity from nose tip	1.374m
final center of gravity from nose tip	1.264m
initial axial moment of inertia	0.1499kg.m^2
final axial moment of inertia	0.1238kg.m^2
initial lateral moment of inertia	41.58kg.m^2
final lateral moment of inertia	33.83kg.m^2
launch velocity	26.7m/s
initial spin rate	2088°/s

IV. SIX DEGREE OF FREEDOM TRAJECTORY MODEL

A computer code is developed which models the flight dynamics of fin stabilized and canard controlled 122mm projectile. The code considers the projectile as a rigid, six degree-of-freedom body and solves the equations of motion in a body coordinate system. The muzzle conditions are used as initial conditions in the calculations. A body-fixed reference frame is chosen for this study since the dynamic behavior of the vehicle is the main object of study. The equations of motion are developed using a body-fixed coordinate system as shown in Fig. 3. The origin of the body axes is the vehicle center of mass, *O*. The angular velocity of the body relative to an inertial frame is $\omega_b(\omega_{bx}, \omega_{by}, \omega_{bz})$ and the components of the translational velocity, V_b in body frame are *(u, v, w)*.

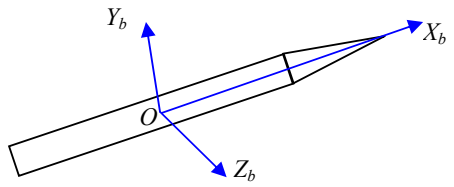

Fig. 3 Orientation of rocket body axes

The earth is treated as spherical and non-rotating in this study since the time of flight for such type of vehicles is of the order of few tens of seconds. Equations used for generating six degree of freedom trajectory model are summarized in the following lines.

$$\dot{u} = -\omega_{by} w + \omega_{bz} v - \frac{Q_D S_r C_A}{m} - \frac{Q S_c C_{Ac}}{m} + \frac{T_{xb}}{m} + G_{xb} \tag{18}$$

$$\dot{v} = -\omega_{bz} u + \omega_{bx} w + \frac{Q_D S_r}{m}\left(C_{N\alpha}\alpha + \frac{\omega_z D C_{N\dot{\alpha}}}{2V_{ab}} \right) + \frac{Q_D S_c C_{N\delta}}{m}(\delta_P + \alpha) + G_{yb} \tag{19}$$

$$\dot{w} = -\omega_x v + \omega_y u + \frac{Q_D S_r}{m}\left(C_{N\beta}\beta + \frac{\omega_y D C_{N\dot{\beta}}}{2V_{ab}} \right) + \frac{Q_D S_c C_{N\delta}}{m}(\delta_Y - \beta) + G_{zb} \tag{20}$$

where δ_P is pitch channel canard deflection angle, δ_R is yaw channel canard deflection angle, $C_{N\alpha}$ is normal aerodynamic force coefficient for rockety body, $C_{N\delta}$ is normal aerodynamic force coefficient due to canards, D is reference diameter of rocket body, S_r is reference area of rocket, S_c is surface area of canard. Dynamic pressure, Q_D, is calculated by the expression

$$Q_D = \frac{1}{2}\rho V_{ab}^2 \tag{21}$$

where V_{ab} is the magnitude of aerodynamic velocity expressed in body frame. V_{ab} is calculated as following

$$\vec{V}_{ab} = \vec{V}_b - \vec{V}_{wb} \tag{22}$$

where $\vec{V}_b$ is the rocket velocity in body frame, with respect to earth, and $\vec{V}_{wb}$ is the wind velocity in body frame. Wind velocity is $\vec{V}_{wb}$ is usually given in local vertical frame(North, East, Down). It has to be transformed to body frame before being used in (22).

Angle of attack α and angle of side slip β, are calculated by using components of $\vec{V}_{ab}$

$$\left|\vec{V}_{ab}\right| = V_{ab} = \sqrt{u_{ab}^2 + v_{ab}^2 + w_{ab}^2} \tag{23}$$

$$\alpha = \tan^{-1}\left(-v_{ab} / u_{ab}\right) \tag{24}$$

$$\beta = \sin^{-1}\left(w_{ab} / V_{ab}\right) \tag{25}$$

With the assumptions in (26) and (27), angular accelerations are given in their simplest form in (28) to (31).

$$I_{xy} = I_{yx} = I_{xz} = I_{zx} = I_{yz} = I_{zy} = 0 \tag{26}$$

$$I_{yy} = I_{zz} \tag{27}$$

$$\dot{\omega}_{bx} = \frac{Q_D S_r D^2 C_{lp}}{2V_a I_{xx}}(\omega_{bx}) + \frac{Q_D S_r D^2 C_{lr}}{2V_a I_{xx}}(\omega_{by}) + \frac{Q_D S_c d_c C_{N\delta}}{I_{xx}}(\delta_R) \tag{28}$$

$$\dot{\omega}_{by} = \frac{Q_D S_r D}{I_{yy}}\left(C_{m\beta}\beta + \left(C_{Nr} + C_{m\dot{\beta}}\right)\left(\frac{\omega_{by} D}{2V_a}\right)\right) - \frac{Q_D S_c x_c C_{N\delta}\left(\delta_Y - \beta\right)}{I_{yy}} - \frac{\left(I_{xx} - I_{zz}\right)}{I_{yy}}\omega_{bx}\omega_{bz} \quad (29)$$

$$\dot{\omega}_{bz} = \frac{Q_D S_r D}{I_{zz}}\left(C_{m\alpha}\alpha + \left(C_{mq} + C_{m\dot{\alpha}}\right)\left(\frac{\omega_{bz} D}{2V_a}\right)\right) + \frac{Q_D S_c x_c C_{N\delta}\left(\delta_P + \alpha\right)}{I_{zz}} - \frac{\left(I_{yy} - I_{xx}\right)}{I_{zz}}\omega_{bx}\omega_{by} \quad (30)$$

I_{xx}, I_{yy}, I_{zz}, I_{xy}, I_{xz}, I_{yx}, I_{yz}, I_{zx}, and I_{zy} are moments of inertia about respective axis. C_{lp} is roll damping moment coefficient, C_{lr} is roll moment coefficient derivative with yaw rate, $C_{m\beta}$ is yawing moment coefficient, C_{Nr} is, $C_{m\alpha}$ is pitching moment coefficient due to angle of attack, C_{mq} is pitching moment coeefeicient due to pitch rate , δ_R is roll channel canrd deflection, d_c is lateral distance between center of pressure of canard and rocket's roll axis, x_c is is longitudinal distance between center of pressure of canard and rocket's centre of gravity. Attitude of the body frame with respect to launch frame is determined by Euler angles θ, ψ and ϕ i.e pitch, yaw and roll respectively. Euler angles are related to angular velocity components of body frame according to the following differential equations.

$$\dot{\phi} = \omega_{bx} + \left(\omega_{by} sin\phi + \omega_{bz} cos\phi\right) tan\psi \quad (31)$$

$$\dot{\psi} = \omega_{by} cos\phi - \omega_{bz} sin\phi \quad (32)$$

$$\dot{\theta} = \frac{\left(\omega_{by} sin\phi + \omega_{bz} cos\phi\right)}{cos\psi} \quad (33)$$

Equations (18) to (20) are integrated to obtain the velocity components of the rocket referred to the body frame. The coordinate transformation is used to determine velocity components of the rocket referred to the launch frame, and since the launch frame is not rotating, these velocity components can be integrated directly to obtain the displacements (rocket position) referred to the launch frame. Following is the matrix for coordinate transformation from body frame to launch frame.

$$T_{BL} = \begin{bmatrix} C\psi C\theta & S\phi S\psi C\theta - C\phi S\theta & C\phi S\psi C\theta + S\phi S\theta \\ C\psi S\theta & S\phi S\psi S\theta + C\phi C\theta & C\phi S\psi S\theta - S\phi C\theta \\ -S\psi & S\phi C\psi & C\phi C\psi \end{bmatrix} \quad (34)$$

C stands for cosine, and S stands for sine function. Velocity vector in launch frame and three differential equations for rocket position in launch frame are given by (35) to (38).

$$\overrightarrow{V_l} = \begin{bmatrix} \dot{x}_l \\ \dot{y}_l \\ \dot{z}_l \end{bmatrix} = T_{BL} \begin{bmatrix} u \\ v \\ w \end{bmatrix} \quad (35)$$

$$\dot{x}_l = C\psi C\theta(u) + \left(S\phi S\psi C\theta - C\phi S\theta\right)(v) + \left(C\phi S\psi C\theta + S\phi S\theta\right)(w) \quad (36)$$

$$\dot{y}_l = C\psi S\theta(u) + \left(S\phi S\psi S\theta + C\phi C\theta\right)(v) + \left(C\phi sin\psi S\theta - S\phi C\theta\right)(w) \quad (37)$$

$$\dot{z}_l = -S\psi(u) + S\phi C\psi(v) + C\phi C\psi(w) \quad (38)$$

V. Trajectory Simulations

Nominal trajectories for the rocket under study have been simulated for launch elevation angles ranging from 30° to 70°. Aerodynamic data for 122mm rocket given in [20] has been used for simulations. A plot of roll rate versus time for launch angle of 50° is shown in Fig. 4(a). Figure 4(b) depicts the plot of rocket altitude versus time, and the plot of altitude versus downrange is shown in Fig. 4(c). It has been observed for all cases of launch angles that the roll rate of rocket damps out to zero within first six seconds of flight owing to the high roll damping moment offered by straight tail fins, to be published [21].

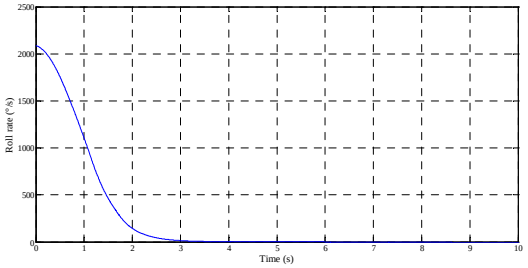

Fig. 4 (a) Roll rate versus time for 50° launch elevation

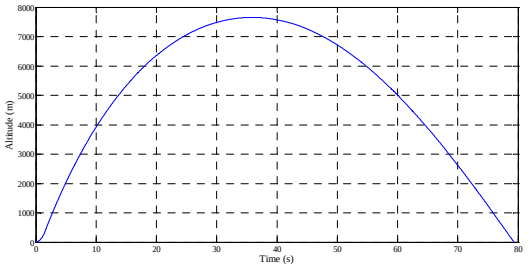

Fig. 4 (b) Rocket altitude versus time for 50° launch elevation

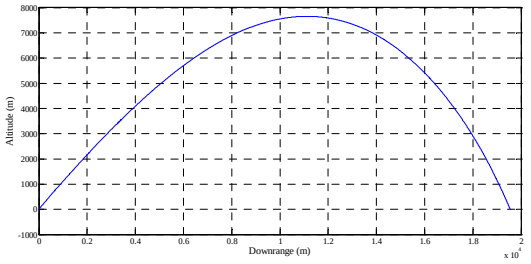

Fig. 4 (c) Rocket altitude versus downrange for 50° launch elevation

Spinning of rocket in the initial phase helps to average out the effects of configurational and mass asymmetries of the rocket, and aids in reducing dispersion. Once the roll rate is zero, the front canards are deployed which can be used for aerodynamic maneuvering in order to execute guidance and control function. Late deployment of canards is adopted in order to avoid unnecessary drag during early part of trajectory that may reduce the effective range of the rocket. After the deployment of canards their foremost function is to bring the roll orientation of rocket to zero degree so that pitch and yaw controls can be appropriately managed at later stages. The next section describes the SDRE model for roll autopilot which generates actuator commands for canard deflection required to orientate the rocket to zero roll position.

VI. SDRE Based Design Model for Roll Autopilot

Roll dynamics of the rocket under study are governed by (39) and (40).

$$\dot{\omega}_{bx} = \frac{Q_D S_r D^2 C_{lp}}{2V_a I_{xx}}\left(\omega_{bx}\right) + \frac{Q_D S_r D^2 C_{lr}}{2V_a I_{xx}}\left(\omega_{by}\right) + \frac{Q_D S_c d_c C_{N\delta}}{I_{xx}}\left(\delta_R\right) \tag{39}$$

$$\dot{\phi} = \omega_{bx} + \left(\omega_{by} sin\phi + \omega_{bz} cos\phi\right) tan\psi \tag{40}$$

In order to develop the SDRE based roll autopilot these equations have to be reformulated to become consonant with the requisite SDRE structure. First we assume decoupled roll, pitch and yaw dynamics leading to following simplified equations for roll dynamics of the rocket.

$$\dot{\phi} = \dot{\phi} \tag{41}$$

$$\ddot{\phi} = \frac{Q_D S_r D^2 C_{lp}}{2V_a I_{xx}}\left(\dot{\phi}\right) + \frac{Q_D S_c d_c C_{N\delta}}{I_{xx}}\left(\delta_R\right) \tag{42}$$

The canard actuator is modeled as a second-order nonlinear system with natural frequency of ω_a = 150rad/s and damping ratio ζ = 0.7. Actuator dynamics are governed by following equations

$$\dot{\delta}_R = \dot{\delta}_R \tag{43}$$

$$\ddot{\delta}_R = -\omega_a^2 \delta_R - 2\zeta\omega_a \dot{\delta}_R + \omega_a^2 \delta_{Rc} \tag{44}$$

where δ_{Rc} is the commanded deflection and δ_R is the actual canard deflection for roll channel.

Complete equations for roll dynamics taking into account actuator dynamics is expressed in state space form consonant with (6) as following

$$\begin{bmatrix} \dot{\phi} \\ \ddot{\phi} \\ \dot{\delta}_R \\ \ddot{\delta}_R \end{bmatrix} = \begin{bmatrix} 0 & 1 & 0 & 0 \\ 0 & \frac{Q_D S_r D^2 C_{lp}}{2V_a I_{xx}} & \frac{Q_D S_c d_c C_{N\delta}}{I_{xx}} & 0 \\ 0 & 0 & 0 & 1 \\ 0 & 0 & -\omega_a^2 & -2\zeta\omega_a \end{bmatrix} \begin{bmatrix} \phi \\ \dot{\phi} \\ \delta_R \\ \dot{\delta}_R \end{bmatrix} + \begin{bmatrix} 0 \\ 0 \\ 0 \\ \omega_a^2 \end{bmatrix} \delta_{Rc} \tag{44}$$

The saturation limits of canard deflection angle and rocket angular rate during the control phase are set to be 30° and 800°/s, respectively. All state variables are assumed onboard measurable. The state weighting matrix Q is chosen to be diagonal as in (45), and the elements are initially selected on the basis of Bryson's rule i.e. every diagonal element of Q should be reciprocal of the square of maximum permissible value of corresponding state, as it provides a good starting point. However, the elements of Q matrix are tailored by trial and error to obtain the appropriate response over the desired operating range which is the flight envelope for the subject rocket in our case. A wide operating range is achieved by making the elements of Q matrix to be state dependent. This makes the state weightings keep on varying at every instance of calculating control action.

$$Q = \begin{bmatrix} q_{11} & 0 & 0 & 0 \\ 0 & q_{22} & 0 & 0 \\ 0 & 0 & q_{33} & 0 \\ 0 & 0 & 0 & q_{44} \end{bmatrix} \tag{45}$$

Following choice of elements of Q matrix gave the control performance within acceptable bounds.

$$q_{11} = \frac{5}{\phi_i^2} - \frac{\phi}{\left(5\phi_i^2\right)} \tag{46}$$

$$q_{22} = \frac{1}{\left(800\right)^2} + \frac{\dot{\phi}^2}{\left(10^9\right)} \tag{47}$$

$$q_{33} = \frac{1}{\left(30^2\right)} \tag{48}$$

$$q_{44} = \frac{1}{\left(800^2\right)} \tag{49}$$

ϕ_i corresponds to the roll orientation of rocket when the roll autopilot starts regulating the roll orientation. The first term of q_{11} remains constant throughout the control process, however the second term keeps on decreasing as the roll error decreases. Keeping the second term of q_{11} as negative helps to avoid large deflection angle of the canard at the start of control process, thereby eliminating the chance of canards going to their saturation limits. Similarly the second term of q_{22} decreases as the roll rate generated due to deflection of canards decreases. Matrix elements q_{33} and q_{44} are chosen as constants to avoid unnecessary computational burden. At the

end of spin phase, the foremost action to be taken by roll autopilot is to nullify the residual roll error/orientation to zero.

During remaining phase of flight the task of the roll autopilot is to keep the roll orientation stabilized to zero roll position and continuously nullify any roll error occurring due to disturbing roll moments. Usually these roll errors are not of high order and remain within one to two tens of degrees. In order to nullify disturbing roll errors, we selected diagonal elements of Q matrix as in (50) to (53).

$$q_{11} = \frac{1}{\phi_i^2} - \frac{Q_D}{\left(3\times 10^7\right)} \tag{50}$$

$$q_{22} = \frac{1}{\left(360\right)^2} + \frac{\dot{\phi}^2}{\left(10^6\right)} \tag{51}$$

$$q_{33} = 0 \tag{52}$$

$$q_{44} = 0 \tag{53}$$

The matrix element q_{11} has been chosen to be a function of initial roll error and dynamic pressure. Since the dynamic pressure depends on altitude and velocity of the rocket, the element q_{11} being function of dynamic pressure enables the autopilot to automatically adjust its performance while performing at different altitudes. As the rocket traverses its trajectory in ascending phase, its velocity and atmospheric density decrease, thereby, reducing the dynamic pressure. This leads to increase in the value of q_{11} at low dynamic pressures and comparatively larger canard deflection is produced to compensate the effect of low aerodynamic force available at low dynamic pressure.

VII. Autopilot Simulation Results

With the above mentioned choice of Q matrix (46) to (49), simulations for SDRE based roll autopilot have been performed for initial roll angles (or residual roll error of spin phase) 90°, 122°, and 150° considering the rocket launch elevation angle to be 50°. During standard trajectory simulations it has been observed that residual roll error of spin phase is about 115° to 125° for launch elevation angles ranging from 30° to 70°, and it is 122° for launch elevation of 50°. We have considered the cases of 90° and 180° initial roll errors as worst case scenarios. Performance of the autopilot is depicted in simulation results shown in Fig. 5 to Fig. 7. The results show that the proposed roll autopilot eliminates 90° roll error in about 0.45 seconds, 122° roll error in 0.6seconds, and 180° initial roll in 0.7seconds. Moreover, the canard deflection angles and roll rates remain well within the prescribed limits. Thus, the proposed roll autopilot successfully performs the task of orientating the rocket to zero roll position soon after the initial spin phase is over.

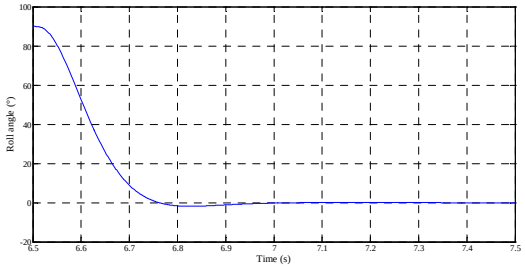

Fig. 5 (a) Roll error decay profile for 90° initial roll error

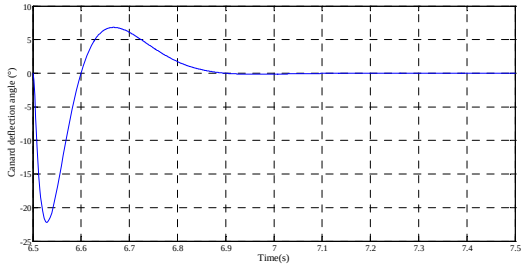

Fig. 5 (b) Canard deflection for correcting 90° initial roll error

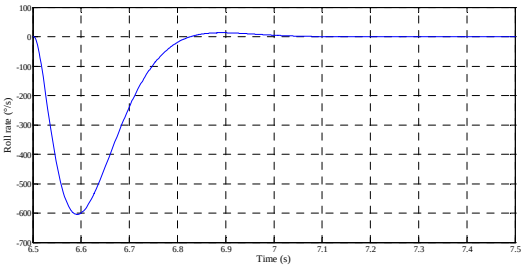

Fig. 5 (c) Roll rate generated for correcting 90° initial roll error

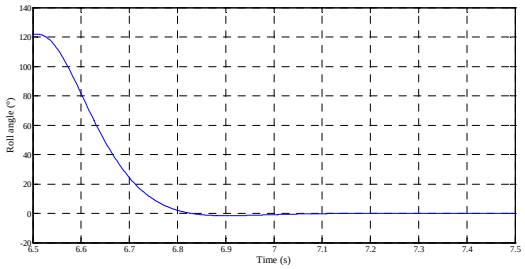

Fig. 6 (a) Roll error decay profile for 122° initial roll error

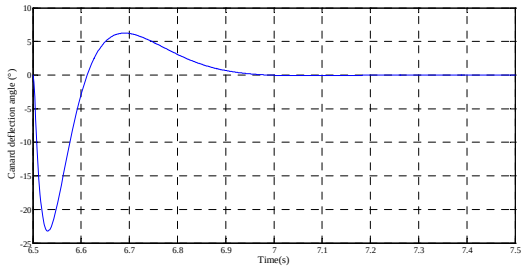

Fig. 6 (b) Canard deflection for correcting 122° initial roll error

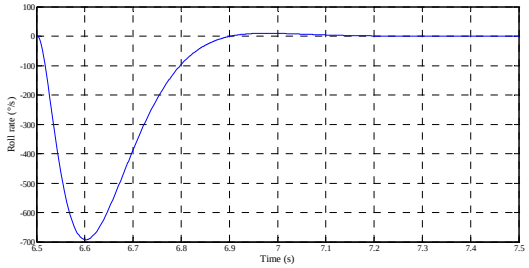

Fig. 6 (c) Roll rate generated for correcting 122° initial roll error

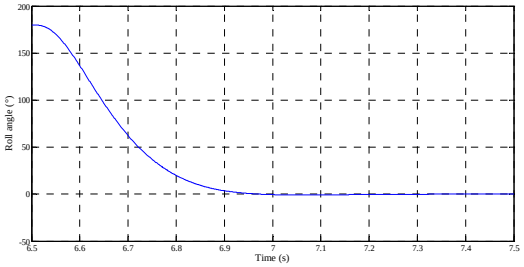

Fig. 7 (a) Roll error decay profile for 180° initial roll error

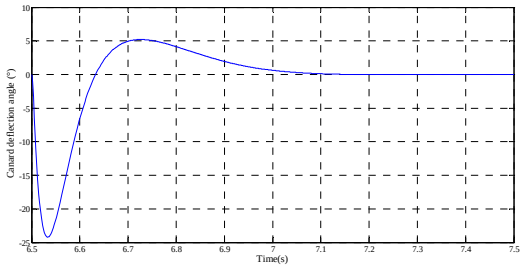

Fig. 7 (b) Canard deflection for correcting 180° initial roll error

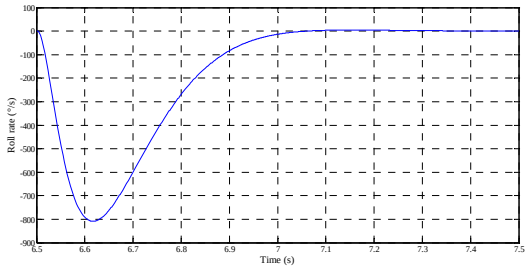

Fig. 7 (c) Roll rate generated for correcting 180° initial roll error

After eliminating the residual roll error of spin phase the roll autopilot keeps the rocket in roll stabilized state at zero degree roll. Performance of the proposed autopilot has also been simulated for 10° roll error at flight altitudes of 4000m, 6000m, and 7500m. The simulation results are presented in Fig. 8 to Fig. 10. The results show that the roll errors are successfully eliminated at different altitudes by the designed autopilot while remaining within performance bounds, thus demonstrating the efficacy of the proposed scheme.

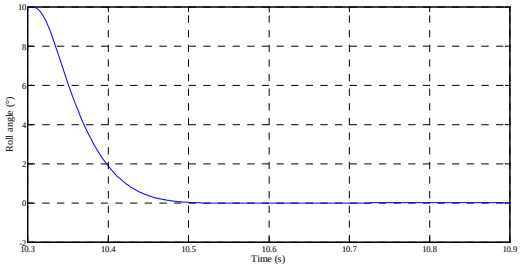

Fig. 8 (a) Roll error decay profile for 10° roll error at 4000m altitude

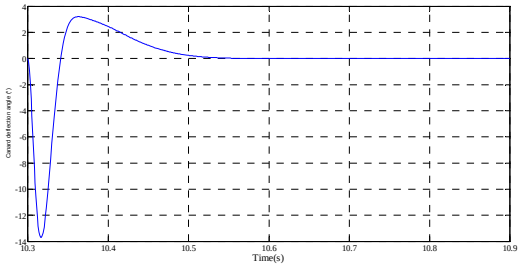

Fig. 8 (b) Canard deflection for correcting 10° roll error at 4000m altitude

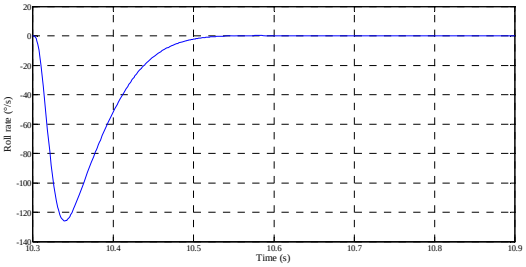

Fig. 8 (c) Roll rate generated for correcting 10° roll error at 4000m altitude

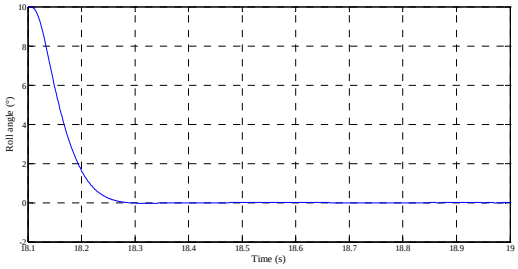

Fig. 9 (a) Roll error decay profile for 10° roll error at 6000m altitude

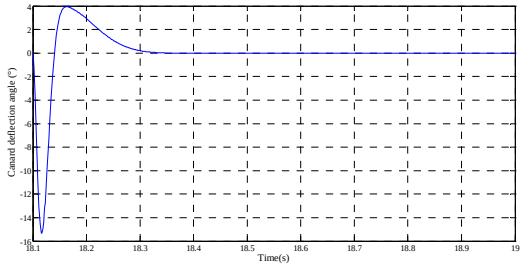

Fig. 9 (b) Canard deflection for correcting 10° roll error at 6000m altitude

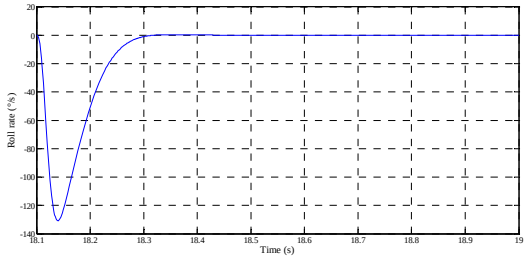

Fig. 9 (c) Roll rate generated for correcting 10° roll error at 6000m altitude

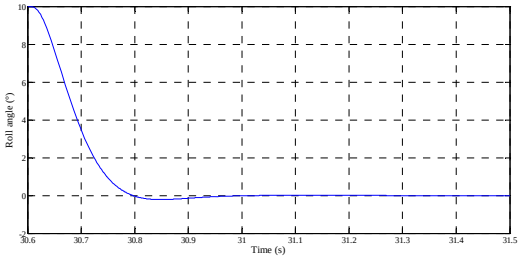

Fig. 10 (a) Roll error decay profile for 10° roll error at 7500m altitude

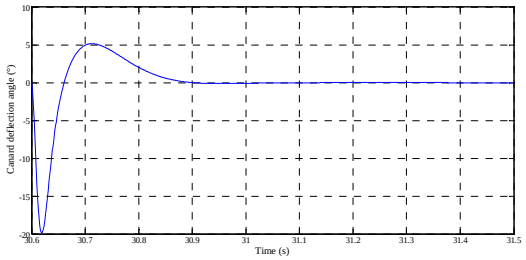

Fig. 10 (b) Canard deflection for correcting 10° roll error at 7500m altitude

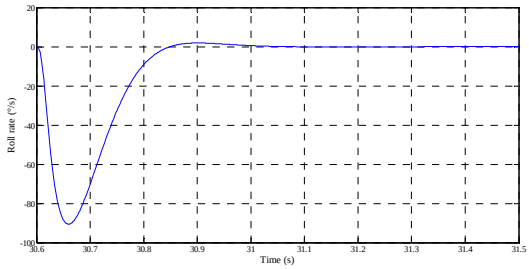

Fig. 10 (c) Roll rate generated for correcting 10° roll error at 7500m altitude

REFERENCES

[1] P. K. Menon, T. Lam, L. S. Crawford, V. H. L. Cheng, and L. Altos, "Real-Time Computational Methods for SDRE Nonlinear Control of Missiles," in *American Control Conference*, pp. 232–237, 2002.

[2] C. P. Mracek and J. R. Cloutier, "Full Envelope Missile Longitudinal Autopilot Design Using the State-Dependent Riccati Equation Method," in *AIAA Guidance, Navigation and Control Conference*, pp. 1697–1705, 1997.

[3] J. R. Cloutier and D. T. Stansbery, "Nonlinear, Hybrid Bank-to-Turn/Skid-to-Turn Missile Autopilot Design," in *AlAA Guidance, Navigation, and Control Conference*, vol. 298, no. 0704, pp. 1–11, 2001.

[4] P. K. Menon, "Integrated Design of Agile Missile Guidance and Control Systems," in *7th Mediterranean Conference on Control and Automation*, pp. 1469–1494, 1999.

[5] A. Ratnoo and D. Ghose, "SDRE Based Guidance Law for Impact Angle Constrained Trajectories," in *AIAA Guidance, Navigation and Control Conference and Exhibit*, no. August, pp. 1–16, 2007.

[6] S. S. Vaddi and P. K. Menon, "Numerical SDRE Approach for Missile Integrated Guidance-Control," in *AIAA Guidance, Navigation and Control Conference and Exhibit*, pp. 1–17, 2007.

[7] E. W. Bogdanov Alexander, "State-Dependent Riccati Equation Control for Small Autonomous Helicopters," *Journal of Guidance, Control, and Dynamics*, vol. 30, no. 1, pp. 47–60, January 2007.

[8] B. A. Steinfeldt and P. Tsiotras, "A State-Dependent Riccati Equation Approach to Atmospheric Entry Guidance," in *AIAA Guidance, Navigation, and Control Conference*, Toronto, 2010, pp. 1–20.

[9] F. Tyan and J. F. Shen, "SDRE Missile Guidance Law," in *8th IEEE International Conference on Control and Automation*, Xiamen, 2010, pp. 866–870.

[10] Tayfun Cimen, "State-Dependent Riccati Equation (SDRE) Control: A Survey," in *17th World Congress, IFAC*, Seoul, 2008, pp. 3761–3775.

[11] Tayfun Cimen, "Survey of State-Dependent Riccati Equation in Nonlinear Optimal Feedback Control Synthesis," *Journal of Guidance, Control, and Dynamics*, vol. 35, no. 4, pp. 1025–1047, 2012.

[12] T. Çimen, "Systematic and effective design of nonlinear feedback controllers via the state-dependent Riccati equation (SDRE) method," *Annual Reviews in Control*, vol. 34, no. 1, pp. 32–51, Apr. 2010.

[13] J. S. Shamma, J. R. Cloutier, E. Air, and F. Base, "Existence of SDRE Stabilizing Feedback," *Aerospace Engineering*, vol. 1, no. 3, pp. 1–14, 2002.

[14] K. D. Hammett, C. D. Hall, and D. B. Ridgely, "Controllability Issues in Nonlinear State-Dependent Riccati Equation Control," *Journal of Guidance, Control, and Dynamics*, vol. 21, no. 5, pp. 767–773, 1998.

[15] A. Bracci, M. Innocenti, and L. Pollini, "Estimation of the Region of Attraction for State-Dependent Riccati Equation Controllers," *Journal of Guidance, Control, and Dynamics*, vol. 29, no. 6, pp. 1427–1430, 2006.

[16] Q. M. Lam, "SDRE Control Stability Criteria and Convergence Issues: Where Are We Today Addressing Practitioners' Concerns?," *in Infotech@Aerospace*, California, 2012, pp. 1–20.

[17] S. Elloumi, I. Sansa, N. B. Braiek, and L. Syst, "On the Stability of Optimal Controlled Systems with SDRE Approach," in *9th International Multi-Conference on Systems, Signals and Devices*, 2012, pp. 1–5.

[18] J. R. Cloutier and D. T. Stansbery, "The Capabilities and Art of State-Dependent Riccati Equation-Based Design," in *American Control Conference*, Anchorage, 2002, pp. 86–91.

[19] S. Katsev, "Streamlining of the State-Dependent Riccati Equation Controller Algorithm for an Embedded Implementation," Rochester Institute of Technology, 2006.

[20] M. Khalil, H. Abdalla, and O. Kamal, "Trajectory Prediction for a Typical Fin Stabilized Artillery Rocket," in *13th International Conference on Aerospace Sciences & Aviation Technology*, Cairo, 2009, pp. 1–14.

[21] M. K. Siddiq, J. C. Fang, W. B. Yu, "Monte Carlo Trajectory Simulations of a Roll Stabilized 122mm Artillery Rocket" in *International Conference on Computer and Electrical Engineering*, Hong Kong, 2012.